

COMPUTATIONAL MULTI-FLUID DYNAMICS PREDICTIONS OF DNB

S. Mimouni

Electricité de France, R&D Division, 6 Quai Watier, 78401 Chatou, France

stephane.mimouni@edf.fr

ABSTRACT

Extensive efforts have been made in the last five decades to evaluate the boiling heat transfer coefficient and the critical heat flux in particular. Boiling crisis remains a major limiting phenomenon for the analysis of operation and safety of both nuclear reactors and conventional thermal power systems. As a consequence, models dedicated to boiling flows have been improved. For example, Reynolds Stress Transport Model, polydispersion and two-phase flow wall law have been recently implemented. In a previous work, we have evaluated computational fluid dynamics results against single-phase liquid water tests equipped with a mixing vane and against two-phase boiling cases. The objective of this paper is to propose a new mechanistic model in a computational multi-fluid dynamics tool leading to wall temperature excursion and onset of boiling crisis. Critical heat flux is calculated against 150 tests and the mean relative error between calculations and experimental values is equal to 8.3%. The model tested covers a large physics scope in terms of mass flux, pressure, quality and channel diameter. Water and R12 refrigerant fluid are considered. Furthermore, it was found that the sensitivity to the grid refinement was acceptable.

KEYWORDS: DNB, critical heat flux, boiling flow

1. INTRODUCTION

When a liquid is flowing onto a heated wall, the heat transferred by the wall to the liquid causes part of the liquid to evaporate, therefore producing a two-phase bubbly flow along the wall. This kind of situation, called the nucleate boiling regime, is an efficient manner to evacuate the heat produced into the wall, for example by Joule effect or by a nuclear reaction. In nucleate boiling, the heat flux increases and reaches a maximum value with increasing surface temperature. Unfortunately, further increase in the surface temperature results in decreasing heat flux as the transition from nucleate boiling to film boiling takes place. The maximum heat flux that can be obtained by nucleate boiling is referred to as the critical heat flux (CHF). In the case of controlled heat flux, a slight increase of heat flux beyond the CHF can cause the surface temperature to rise to a value exceeding the surface material's maximum allowable temperature. This in turn can cause severe damage or meltdown of the surface.

As a consequence, CHF has been extensively studied in the last five decades, as a major limiting phenomenon for nuclear power plant capabilities, as well as in other industries.

The scope of the present work is limited mostly to the boiling crisis in subcooled-flow boiling, which is of interest in the design of fuel assemblies used in nuclear fission, pressurized water reactors (PWR). This kind of situation is named departure from nucleate boiling (DNB).

To predict CHF, many empirical correlations have been developed as well as a few theoretical models. Although empirical correlations can be very reliable in the range of conditions where they have been

established, their use outside this domain is very hazardous. On the contrary, theoretical models, by taking into account the basic mechanisms involved in the CHF phenomenon, should better adapt to any new flow boiling configuration.

This paper is organized as follows. In section 2 the general model we use for two-phase boiling flow simulations is presented. In section 3, previous work about validation for adiabatic bubbly flows and boiling flows is summed up. Section 4 is dedicated to validation of DNB tests in a tube. Finally, conclusions are drawn about our current capabilities to simulate DNB and perspectives for future work are given.

2. PHYSICAL MODELLING

2.1 Introduction

The CFD code NEPTUNE_CFD is a three-dimensional, two-fluid code developed for two-phase flows and more especially for nuclear reactor applications. This CFD code is based on the classical two-fluid one pressure approach, including mass, momentum and energy balances for each phase.

The NEPTUNE_CFD solver, based on a pressure correction approach, is able to simulate multi-component multiphase flows by solving a set of three balance equations for each field (fluid component and/or phase) [12]. These fields can represent many kinds of multiphase flows: distinct physical components (e.g. gas, liquid and solid particles); thermodynamic phases of the same component (e.g.: liquid water and its vapour); distinct physical components, some of which split into different groups (e.g.: water and several groups of different diameter bubbles); different forms of the same physical components (e.g.: a continuous liquid field, a dispersed liquid field, a continuous vapour field, a dispersed vapour field). The solver is based on a finite-volume discretization, together with a collocated arrangement for all variables. The data structure is totally face-based, which allows the use of arbitrary shaped cells (tetrahedra, hexahedra, prisms, pyramids, ...) including non conforming meshes.

2.2 Governing equations

The CFD module is based on the two-fluid approach [14-4]. In this approach, a set of local balance equations for mass, momentum and energy is written for each phase. These balance equations are obtained by ensemble averaging of the local instantaneous balance equations written for the two phases. When the averaging operation is performed, the major part of the information about the interfacial configuration and the microphysics governing the different types of exchanges is lost. As a consequence, a number of closure relations (also called constitutive relations) must be supplied for the total number of equations (the balance equations and the closure relations) to be equal to the number of unknown fields. We can distinguish three different types of closure relations: those which express the inter-phase exchanges (interfacial transfer terms), those which express the intra-phase exchanges (molecular and turbulent transfer terms) and those which express the interactions between each phase and the walls (wall transfer terms).

The forces exerted on bubbles are the averaged drag, added mass, lift and turbulent dispersion forces.

Concerning the turbulent transfer terms, the $K - \varepsilon$ model and the RSTM model have been extensively validated in our previous work in simple as well as complex geometries [22-23-24-25-26]. For flows encountered in vertical pipes, similar results have been obtained with both models.

As the turbulent heat flux is directly proportional to $v_l^T = C_\mu \frac{K_l^2}{\varepsilon_l}$; (v_l^T is the liquid turbulent eddy viscosity, K_l is the liquid turbulent kinetic energy, and ε_l its dissipation rate), and the thermal layer at the

wall turns out to be of interest, it needs to be carefully calculated. As a consequence, both turbulence models will be tested in the following.

The bubble size distribution modelling has been developed for bubbly flow based on the moment density method [30], where we assume that all the bubbles have the same velocity and the same temperature despite possibly different diameters.

2.3 Wall function for boiling flow

In subcooled flow boiling, the liquid velocity profile in the boundary layer is significantly disturbed by the bubble formation and detachment mechanisms on the heated wall. In the literature, an over-prediction of liquid and gas velocity distributions in the boiling boundary region has been reported. The use of single-phase wall law may be one of the main reasons for these results. Following Roy et al. [29], Gabillet et al. [8] and Ramstorfer et al. [28], Mimouni et al. [23] suggested a wall function for boiling flows. When the void fraction tends to zero, the wall law tends to the single-phase formulation. Furthermore, this relation depends on bubble diameter and bubble density at the wall (void fraction at the wall), which is physically expected. This formulation proved to be a key point in the CHF simulation.

2.4 Wall transfer model for nucleate boiling

The CHF phenomenon has received considerable attention in the past, and different mechanisms have been proposed to interpret its cause.

Weisman and Pei [33] assume that DNB appears when a thin layer adjacent to the wall reaches a limiting bubble concentration due to the inability of the main stream to remove the bubbles, because the turbulent eddies are too small to influence the bubble trajectories. The critical void fraction in the layer corresponds to a maximum packing of bubbles and is estimated at 82%.

Lee and Mudawwar [19] postulate that small vapour blankets are formed due to the piling of bubbles flowing along the wall after their departure. A dry spot may appear when the vapor blanket length is such that a Helmholtz instability of the liquid-vapor interface occurs. DNB is then assumed to appear when the vaporization rate overcomes the liquid flow in the sublayer.

In the present paper, in a first, simplified approach, and following the analysis of Kurul et al. [16], the boiling heat flux is split into three terms:

- a single-phase flow convective heat flux q_c at the fraction of the wall area unaffected by the presence of bubbles,
- a quenching heat flux q_q from bubbles departing from the wall and bringing cold water in contact with the wall periodically,
- a vaporisation heat flux q_e needed to generate the vapour phase.

The basic wall heat flux partitioning model assumes that the amount of water on the wall is sufficient to remove heat from the wall and to be used for evaporation. Superheating of the vapour that occurs at high void fractions is not modelled. Given all this, the basic heat flux partitioning model cannot be used under critical heat flux conditions. In order to take into account the phenomenon of temperature excursion at DNB conditions, the heat flux partitioning model has been generalized by adding a fourth part of the wall heat flux, q_v , diffusive heat flux used to superheat the gas phase:

$$q_v = h_{vap}(T_{wall} - T_v),$$

where h_{vap} is the wall heat transfer coefficient calculated from the temperature wall function for the vapour phase, T_v is the vapour temperature at the centre of the wall-adjacent cell. Thus, the heat flux imposed at the wall is written as :

$$q_{wall} = f_{al}(q_c + q_q + q_e) + (1 - f_{al})q_v \quad [W / m^2]$$

Where f_{al} is a phenomenological function, which depends on the liquid volume fraction α_l and takes care for the numerically smooth transition between the nucleate boiling regime and the CHF regime. More details can be found in [27].

The critical value for the void fraction is $1 - \alpha_{l,crit} = 0.82$. The local void fraction equal to 0.82 can be used as a criterion for the CHF occurrence. Actually, this formulation can be considered as a transcription of the Weisman DNB criterion in a CFD code [33].

If we apply the simple criterion above, the void fraction in the nearest cell at the wall strongly depends on the mesh size as the vapour production at the wall is a function of the liquid temperature and velocity.

To ensure grid independence, the liquid temperature T_l in wall boiling equations is calculated from the logarithmic temperature profile at the given non-dimensional distance from the wall $y^+ = YPLUS$ rather than from the centre of the wall-adjacent cell.

This approach is valid only if the wall-adjacent cells remain in log region of the wall boundary layer ($30 < y^+ \leq 300$). The same process is applied to the liquid velocity. The Weisman DNB criterion is applied to the void fraction calculated at $y^+ = YPLUS$.

Moreover, if the liquid temperature in the nearest cell at the wall tends to the saturation temperature, then the single-phase-flow convective heat flux q_c tends to 0, and the corresponding energy contributes to the vaporisation heat flux. This modification of the initial wall transfer model for nucleate boiling turns out to be crucial : if the heat flux imposed at the wall is large enough (which is the case under DNB conditions), then the vaporisation heat flux tends to the heat flux imposed at the wall, which means that vapor production at the wall is correctly predicted and that the correlations, source of discrepancies, for the density sites and so on have lesser and lesser influence on the results. This theory is supported by experimental results: Chichoux [3] and Garnier [9] have used two different materials in DEBORA test cases under critical heat flux conditions and the material proved to have no influence on the results; as the site density depends on the material surface, as a consequence, a DNB model should be independent of the site density.

We will see in the following that the Weisman DNB criterion is not sufficient and fails in 50% of the cases. As a consequence, the Weisman DNB criterion is reinforced by considering not only the void fraction but also the liquid temperature calculated at $y^+ = YPLUS$ [27].

3. VALIDATION FOR ADIABATIC BUBBLY FLOWS AND BOILING FLOWS

Since the maturity of two-phase CFD has not reached yet the same level as single phase CFD, an important work of model development and thorough validation is needed. Many of these applications involve bubbly and boiling flows, and therefore it is essential to validate the software on such configurations. In particular, this is crucial for applications to flow in PWR fuel assemblies, including studies related to DNB. Four experiments were selected for the validation. The Liu and Bankoff experiment [20] is an adiabatic air-water bubbly flow inside a vertical pipe. It allows to validate forces applied to the bubbles. The Bel F'Dhila and Simonin [2] experiment is an adiabatic bubbly air-water flow inside a sudden pipe expansion. It allows to validate the dynamic models and turbulence. The DEBORA [21] and the ASU [29] facilities provide results for boiling flows inside a vertical pipe. The working fluid is refrigerant R12 for DEBORA and R113 for ASU. Both allow to validate the nucleation modeling on a heated wall, and ASU allows also the validation of the two-phase wall function [22-23-24-25-26]. A key

feature of this work is that all these computations were performed with a single and consistent set of models. Douce et al. [7] have shown that the physical models implemented in NEPTUNE_CFD have captured experimental profiles with reasonable accuracy.

4. CALCULATIONS OF DNB TESTS IN A TUBE

Among various tests, we have selected mostly negative-quality (at the outlet) tests such that the condensation effects dominate coalescence / break up effects, the modelling of which is far from being reliable today. As a consequence, the bubble diameter drops with distance from the wall.

4.1 Calculation procedure

The Russian Academy of Sciences produced a series of standard tables of CHF as function of the bulk mean water condition and for various pressures and mass velocities for a fixed tube diameter of 8 mm [11].

Table I: Experimental conditions retained for DNB tests in an 8 mm tube

CHF MW/m ²	Subcooling (K) at the outlet					
		75	50	25	10	0
Mass velocity kg/m ² s	2000		4.50	3.65	3.00	2.45
	2500		5.05	4.05	3.35	2.65
	3000	6.80	5.65	4.45	3.60	2.85
	4000	8.30	6.70	5.25	4.25	3.15
	5000	9.80	7.85	5.90	4.70	3.75

For tube diameters other than 8 mm, the CHF is given by the approximate relationship:

$$CHF = CHF_{8mm} \sqrt{\frac{8}{D_{tube} [mm]}} \text{ for } D_{tube} \text{ between 4 and 16 mm.}$$

The flow is assumed to be axisymmetric; therefore a two-dimensional axisymmetric meshing is used.

The calculation is started with the wall heat flux equal to 70%CHF. The wall heat flux is then increased by 5% progressively. After each step, the wall heat flux reaches a plateau in order to stabilise the boiling flow. This procedure is repeated until the wall heat flux is equal to 130%CHF. In the calculations, CHF is detected when the wall temperature exceeds 1000K (Figure 1). In fact, the zircaloy clad tubes start to degrade at about 1000K. Because of the sudden rise in temperature, results are weakly sensitive to the wall temperature chosen for CHF detection. The relative error is evaluated in each case, and the mean relative error and the standard deviation is calculated in each set of computations. When the CHF is not detected (i.e. > 30%) by the CFD tool, then the relative error is assumed to be equal to 100%.

4.2 Sensitivity to the mesh refinement

Computations have been performed on three kinds of meshing: a coarse grid, a medium grid and a fine grid (table II). Results are similar below the DNB value calculated by the code (Figure 1). But, the DNB value calculated can differ from the coarse grid to the fine grid. The sensitivity to the mesh refinement has been tested in 23 cases (table 1) and the results are summarized in table III: the sensitivity to the mesh refinement proves to be acceptable. Figure 2-Figure 4 give a view of the results. Hence the subsequent

calculations are performed on the medium grid.

Table II: Definition of the grids

Mesh size (mm)	Coarse grid	Medium grid	Fine grid
Radial direction	1	0.5	0.25
Axial direction	10	5	2.5

Table III: Mean relative error and standard deviation vs. mesh refinement

%	Mean relative error	Standard deviation
Coarse grid	-4.5	4.3
Medium grid	-8.6	3.6
Fine grid	-1.7	6.2

4.3 Sensitivity to the tube diameter and to the turbulence modelling

In contrast to empirical relations, theoretical models implemented in the CFD code that take into account the basic mechanisms involved in the CHF phenomenon, should better adapt to any new flow boiling configuration and to geometry. Thus, the DNB model is assessed in a large scope in terms of mass flux, pressure, quality and channel diameter in this section. Figure 5-Figure 9 represent the CHF calculated vs the experimental value for the 23 cases defined in table 1 and for tube diameters between 6 and 10 mm. Findings are summarized in table IV and we note that the use of R_{ij} - ϵ turbulence model divides the error by at least a factor of two.

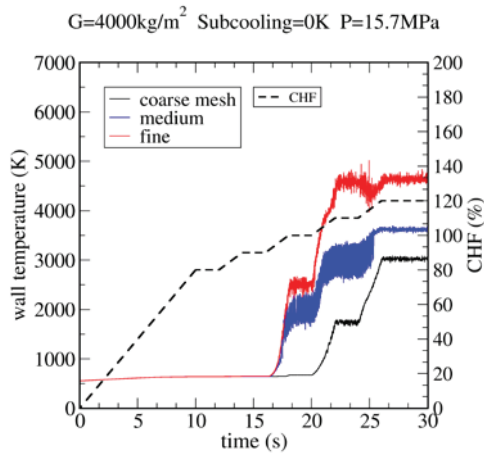


Figure 1: Sensitivity to the mesh refinement – wall temperature plotted against heat flux imposed at wall

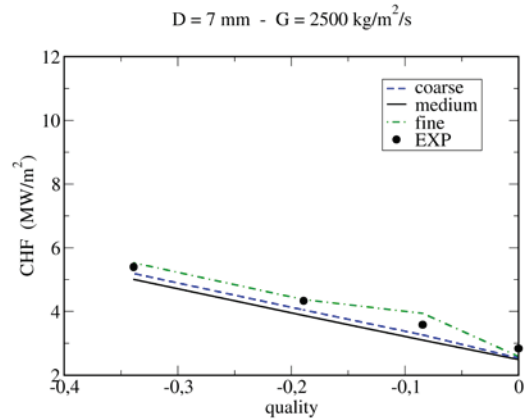


Figure 2: Sensitivity to the mesh refinement, mass flowrate = 2500 kg/m²/s

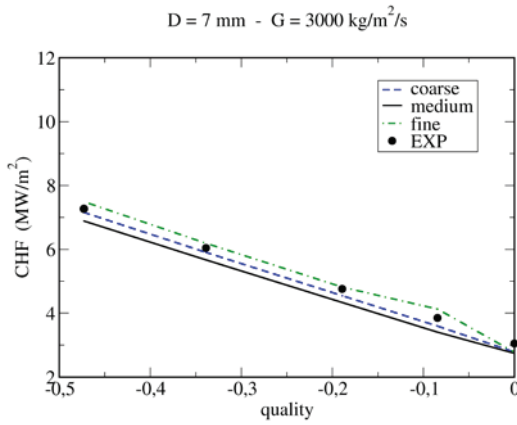


Figure 3: Sensitivity to the mesh refinement, mass flowrate = 3000 kg/m²/s

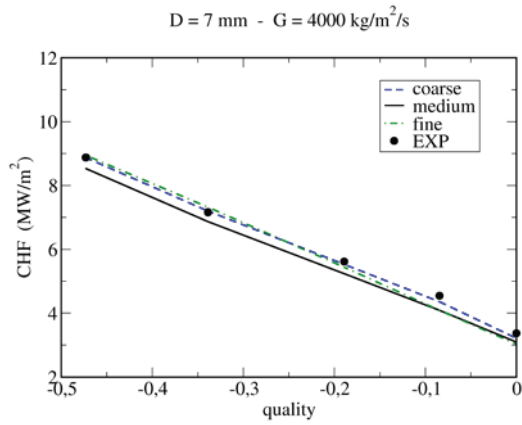


Figure 4: Sensitivity to the mesh refinement, mass flowrate = 4000 kg/m²/s

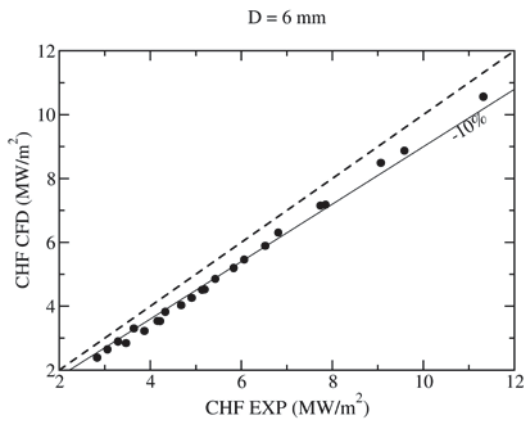


Figure 5: CHF calculated vs experimental CHF, tube diameter = 6 mm

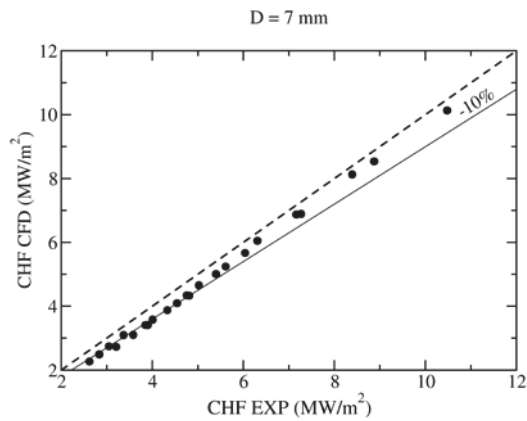


Figure 6: CHF calculated vs experimental CHF, tube diameter = 7 mm

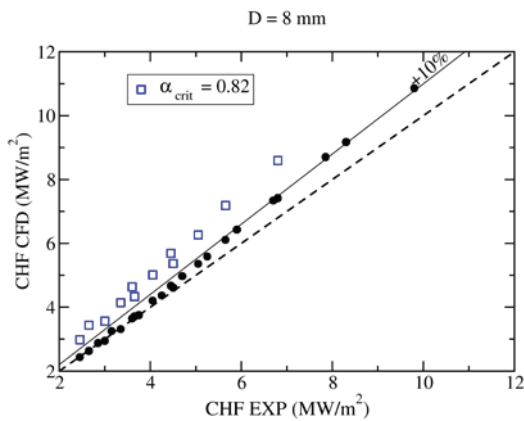


Figure 7: CHF calculated vs experimental CHF, tube diameter = 8 mm

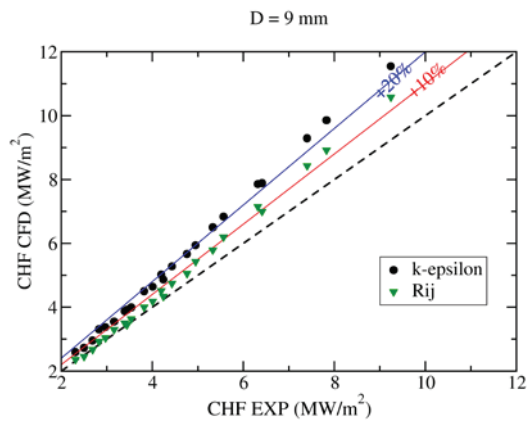


Figure 8: CHF calculated vs experimental CHF, tube diameter = 9 mm

Table IV: Mean relative error and standard deviation vs. tube diameter and turbulence modelling

%	Mean relative error	Standard deviation
Dtube= 6 mm	-11.5	3.4
Dtube= 7 mm	-8.6	3.6
Dtube= 8 mm	4.4	4.2
Dtube= 8 mm, Weisman	60.4	38.9
Dtube= 9 mm	17.8	5.1
Dtube= 9 mm, Rij-ε	6.1	4.9
Dtube= 10 mm	30.7	5.7
Dtube= 10 mm, Rij-ε	17.2	5.5

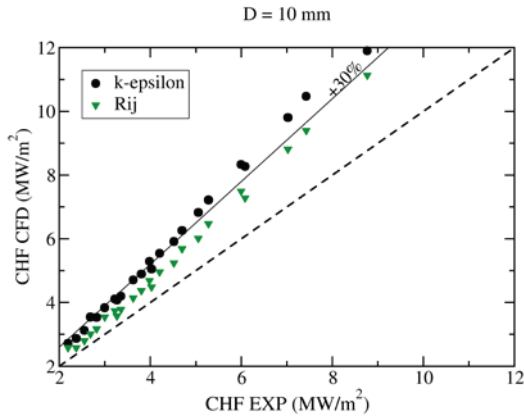


Figure 9: CHF calculated vs experimental CHF, tube diameter = 10 mm, sensitivity to the turbulence model

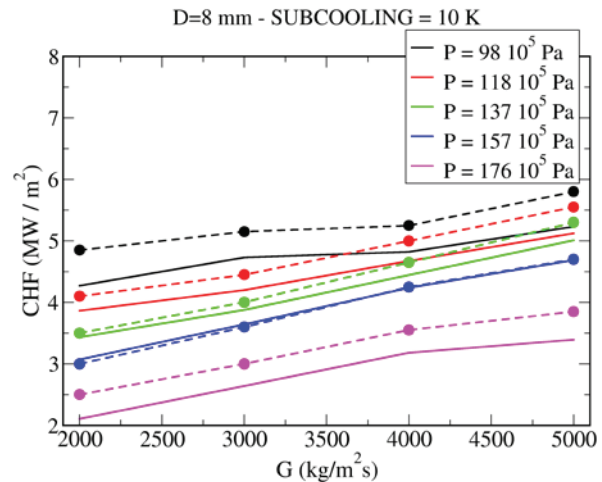


Figure 10: CHF prediction for different pressure values.

4.4 Sensitivity to the pressure

In order to complete the validation of the previous section, we keep constant the value of the subcooling equal to 10K and we study the sensitivity to pressure. The experimental conditions retained are given in table V. Figure 10 shows good agreement between calculations and experimental data, confirmed by a mean relative error of 7.2% and a standard deviation of 4.8%.

TableV: Experimental conditions retained for the sensitivity to the pressure

CHF MW/m2	Pressure (MPa)					
	17.6	15.7	13.7	11.8	9.8	
Mass velocity kg/m2s	2000	2.5	3.00	3.50	4.10	4.85
	3000	3.00	3.60	4.00	4.45	5.15
	4000	3.55	4.25	4.65	5.00	5.25
	5000	3.85	4.70	5.30	5.55	5.80

4.5 Weisman criterion

The Weisman criterion has been improved in order to reach a weak sensitivity to the mesh refinement and to the wall transfer model for nucleate boiling. Once more again, the 23 cases defined in table 1 have been calculated. Figure 7 shows that boiling crisis was detected in only 50% of the cases with a value degraded when comparing to the DNB model proposed in the

paper. Figure 11 shows that the void fraction does not reach the value of 0.82 in most of cases. Thus, the Weisman criterion can not be used as a DNB criterion in the CFD tool (table VI).

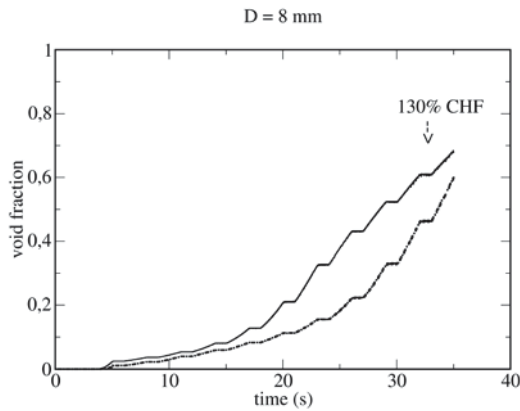


Figure 11: Void fraction at the nearest cell at the wall located at the CHF elevation

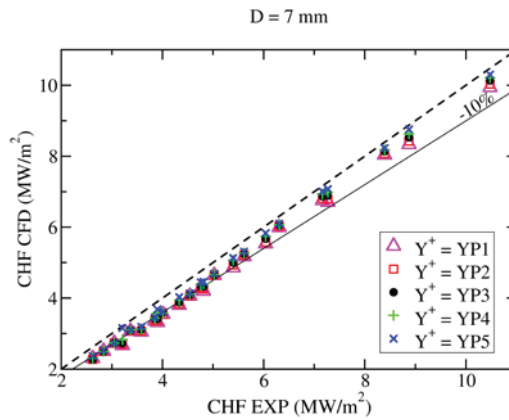


Figure 12: CHF calculated vs experimental CHF, tube diameter = 7 mm, sensitivity to Y^+

Table VI: Mean relative error and standard deviation vs. DNB model

%	Mean relative error	Standard deviation
Dtube= 8 mm, Weisman	60.4	38.9
Dtube= 8 mm	4.4	4.2
All cases	8.3	4.2

4.6 Sensitivity to the normalized values of wall distance y^+

The logarithmic wall function describes the velocity and the temperature profiles of the turbulent flow close to the wall. This function is valid only for bounded values of y^+ . The 23 cases defined in table 1 have been calculated to assess the sensitivity to the non-dimensional wall distance y^+ . Figure 12 and Table VII show that results are similar for y^+ values between 100 and 300 and the mean relative error remains acceptable. As a consequence, y^+ is fixed to 200 in all computations.

Table VII: mean relative error and standard deviation vs. Y^+

%	Mean relative error	Standard deviation
Dtube= 7 mm, $Y^+ = YP1 = 100$	-9.9	3.4
Dtube= 7 mm, $Y^+ = YP2 = 150$	-9.3	3.5
Dtube= 7 mm, $Y^+ = YP3 = 200$	-8.6	3.6
Dtube= 7 mm, $Y^+ = YP4 = 250$	-7.6	3.3
Dtube= 7 mm, $Y^+ = YP5 = 300$	-6.1	3.3

4.7 Saturated cases

According to the previous sections, the calculated values of CHF turn out to be in reasonable agreement with experimental values for a large scope in terms of mass flux, pressure, and channel diameter. Nevertheless, given the intended applications, only subcooled cases have been considered. In this section, we test 10 saturated cases with a quality slightly positive. The experimental conditions retained are presented in table VIII.

In CHF tables, DNB data points are not distinguished from dryout data points. The generalized boiling model presented in this work assumes bubbly flow with a DNB-type of boiling crisis.

Using this model for dryout data points is not physically meaningful. Therefore, it is necessary to select only DNB data points for the simulations. Unfortunately, it is not completely clear how to distinguish between the two types of boiling crisis. The transition from slug/churn to annular flow can be determined by the approach of Taitel : the data points selected in table VII, are DNB-type of boiling crisis.

Figure 13 represents the calculated values plotted against the experimental values of CHF. The mean relative error is 3.6% which suggests that the boiling crisis model proposed in the paper could be extended to saturated cases.

Figure 13 summarizes the results for tube diameter equal to 8 mm. CHF is plotted against mass flowrate and for several values of quality (X). Discrepancies seem to increase for high CHF values. Indeed, the wall heat flux is increased by 5% progressively and maintained constant until a stationary state is reached. If the CHF = 1 MW/m², the wall heat flux step is equal to 0.05 MW/m² but equal to 0.5 MW/m² for CHF=10 MW/m² which leads to a coarse discretization regarding the wall heat flux.

As a consequence, high CHF values are less well predicted.

CHF MW/m ²	quality		
		0.05	0.1
Mass velocity kg/m ² s	2000	2.1	1.75
	2500	2.2	1.8
	3000	2.25	1.85
	4000	2.6	2.1
	5000	3	2.4
Mean relative error	3.6		
Standard deviation	1.9		

Table VIII: Experimental conditions retained for CHF tests in a 8 mm tube and results

Pinlet (MPa)	Poutlet (MPa)	G (kg/m ² /s) Mass flowrate	Liquid temperature (°C) at inlet
3.10	3.02	2992	21.1
3.09	3.00	4001	32.5
3.11	3.01	5005	37.0
3.08	3.01	2012	36.6

Table IX: Experimental conditions retained for DEBORA tests

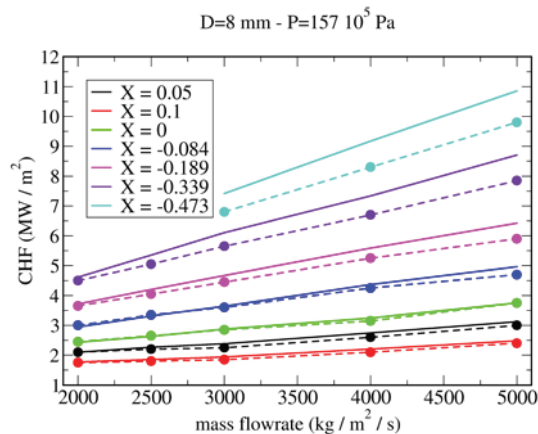
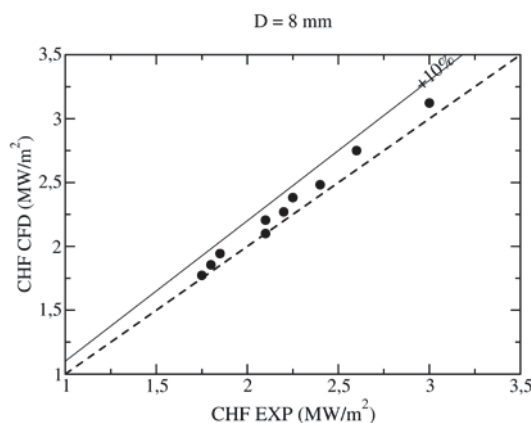


Figure 13: CHF calculated vs experimental CHF for several values of outlet quality.

4.8 Sensitivity to the working fluid

Tests were performed on the DEBORA loop at CEA-Grenoble with R12 refrigerant as a cooling fluid [21]. Global flow data are given in Table IX. The calculation domain is a vertical cylindrical tube of 19.2 mm internal diameter and 3.485 m heated length

Results are presented in Figure 14 and the mean error is less than 10% which is very encouraging.

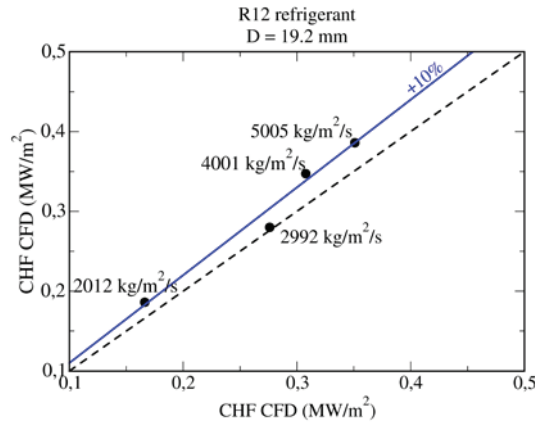


Figure 14: CHF calculated vs experimental CHF for R12 refrigerant fluid

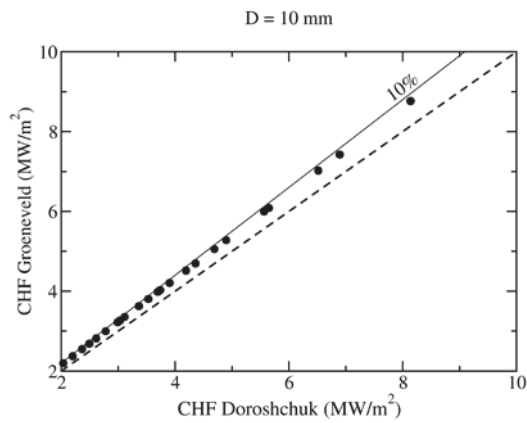


Figure 15: Groeneveld vs Doroshchuk CHF values

4.9 CHF tables

All CHF look-up tables present CHF values at discrete ranges of pressure, mass flux and quality for 8 mm tubes. A correction factor for CHF is used to account for the diameter effect and to extend the applications to other values of tube diameter. Doroshchuk et al. [6] corrected their tabulated CHF values with the diameter ration

$$CHF = CHF_{8mm} \left(\frac{8}{D_{tube} [mm]} \right)^n$$

where CHF is the CHF value for a diameter of interest and CHF_{8mm} is the CHF value for a 8 mm tube (i.e. from the CHF table). D_{tube} is the tube diameter value in mm. Doroshchuk et al suggested a value of 1/2 for the exponent n whereas Groeneveld et al. found a better agreement with $n=1/3$. Figure 15 shows the discrepancies for a 10 mm tube between $n=1/2$ and $n=1/3$. The mean relative error is about 8%. For a 8 mm diameter tube, the mean relative error calculated with our DNB model is 4.4% whereas is equal to 17.2 with a 10 mm tube. It seems that the discrepancies calculated for tube diameter greater than 8 mm are due in part to the value of n . This assumption is reinforced by Figure 14 where the discrepancies do not exceed 8% for a 19.2 mm tube.

As a consequence, if we consider only tube diameter values around 8 mm (i.e. 7 and 9mm), the mean relative error is about 6% which is lower than the error due to the correction factor to account for diameter effect. Thus, the DNB model proposed in the paper turns out to be of relevant interest, and is validated against 150 validation cases and tested on 355 cases.

4.10 Sensitivity to the modelling of forces exerted on bubbles

In the latest version of the NEPTUNE CFD code, boiling cases are systematically validated using the same set of models regarding forces exerted on bubbles and the second-order turbulence model. In this section, the lift force is the Tomiyama lift force [31] and the added mass force is the one by Zuber [34]. The liquid turbulence model is an adaptation to the SSG model dedicated to two-phase flow. As described above, 23 cases have been performed in a tube of diameter 7 mm with the thermal-hydraulic conditions of table 1. Some results are shown in Figure 16. The main result is that the detection of the CHF occurrence can be improved by considering the evolution of the evaporation heat flux: a continuous drop seems to be the best efficient indicator. For these 23 cases, we see that the CHF mean value evaluated by the evaporation heat flux criterion and by the wall temperature (which must exceed 1000K) improve the CHF predictions. The sensitivity to the mesh refinement has also been tested. As already noted, the standard model without CHF criteria fails to predict the DNB occurrence.

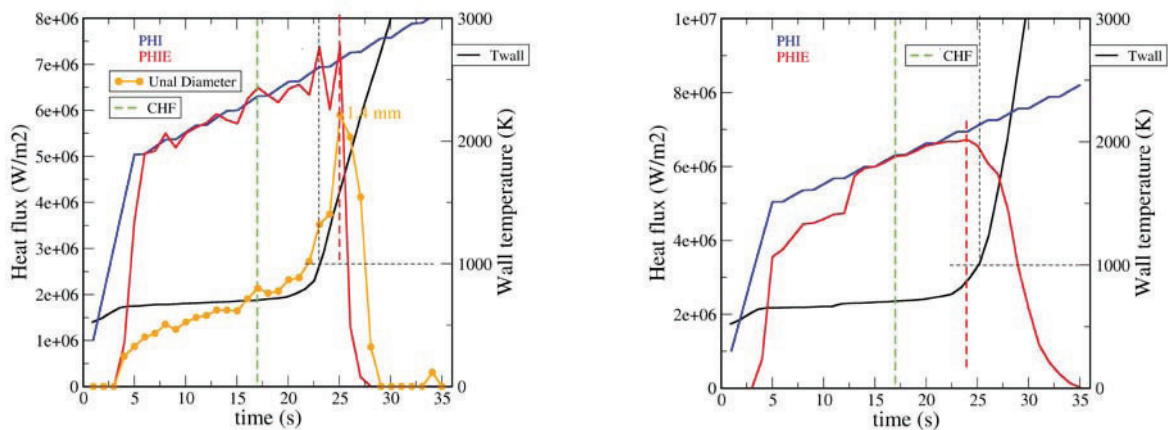
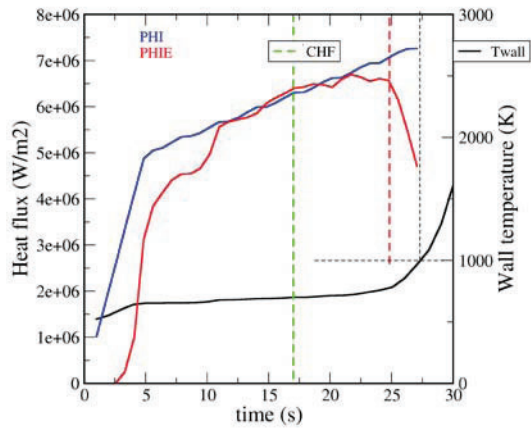


Figure 16: mass flowrate = 5000 kg/s/m² and subcooling = 25 K. Top left : coarse mesh, Top right : fine mesh, bottom : standard mesh.

**PHI = total heat flux imposed at the wall.
 PHIE = evaporation heat flux.
 Unal Diameter : detachment bubble diameter.**



5. CONCLUSION AND PERSPECTIVES

In the framework of the nuclear industry, a CFD tool has been developed and advanced models dedicated to boiling flows have been implemented and validated against experimental data for ten years now including a wall law for boiling flows, wall heat transfer for nucleate boiling, turbulence and a polydispersion model. A mechanistic modelling of CHF taking into account all

the technical results and the experience gained was investigated in this work. Calculations have been performed on 150 experimental cases covering a large physics scope in terms of mass flux, pressure, quality and channel diameter, including four supplementary cases with R12 refrigerant fluid. Wall temperature excursion and onset of boiling crisis are reasonably well reproduced whereas the mean relative error between calculations and experimental values is equal to 8.3% and is partly due to the discrepancies of the diameter correction term used in tabulated CHF values. The standard deviation is particularly small which seems to indicate that basic mechanisms involved in the CHF phenomenon are correctly reproduced. The authors are aware that validation in pipe flow are far from being sufficient and validation work should continue to further evaluate the DNB model and improve it, in particular in complex geometries.

ACKNOWLEDGEMENTS

This work has been performed in the framework of the NEPTUNE project, financially supported by CEA (Commissariat à l'Énergie Atomique et aux Energies Renouvelables), EDF, IRSN and AREVA-NP.

REFERENCES

1. T.R. Auton, "The lift force on a spherical body in a rotational flow", *J. Fluid Mech.*, Vol. **183**, pp. 199-218 (1987).
2. R. Bel F'Dhila, O. Simonin, "Eulerian prediction of a turbulent bubbly flow downstream of a sudden pipe expansion", *Proc. 6th Workshop on Two-Phase Flow Predictions*, 30 mars-2 avril, Erlangen (1992).
3. Ch. Chichoux, "Essais de crise d'ébullition en tube 19,2mm, acier inoxydable 316 TI, longueur chauffante 3,5m", CEA internal report, DRN/DTP/STR/LETC/93-132, in French.
4. J-M. Delhaye, M. Giot, and M.L. Riethmuller, M. L., "Thermal-hydraulics of two-phase systems for industrial design and nuclear engineering", Hemisphere and McGraw Hill, 1981.
5. R. Denèfle, S. Mimouni, J.-P. Caltagirone, S. Vincent, "Hybrid multifield method applied to bubble rising and coalescence", *Int. Jr. of Computational Methods and Experimental Measurements* vol. **2**, n°1 (2014).
6. V.E. Doroshchuk, L.L. Levitan, F.P. Lantzman, "Investigation into burnout in uniformly heated tubes", *ASME publication 75-WA HT-22*, 1975.
7. Douce, S. Mimouni, M. Guingo, C. Morel, J. Laviéville, C. Baudry, "Validation of NEPTUNE_CFD 1.0.8 for adiabatic bubbly flow and boiling flow", submitted to Nuclear Engineering and Design.
8. Gabillet, C., Colin, C., Fabre, J., "Experimental study of bubble injection in a turbulent boundary layer", *Int. J. Multiphase Flow* **28**, pp. 553-578 (2002).
9. J. Garnier, "Essais de crise d'ébullition en tube 19,2 mm", CEA internal report, DRN/DTP/STR/LETC/91-45, in French.
10. J. Garnier, "DEBORA : Topologie d'écoulement : mise en forme et description de la banque finalisée", CEA report number SETEX/LDF/98-65 (1998), in French.
11. D.C.Groeneveld, L.K.H. Leung, P.L. Kirillov, V.P. Bobkov, I.P. Smogalev, V.N. Vinogradov, X.C. Huang, E. Royer, "The 1995 look-up table for critical heat flux in tubes", *Nuclear Engineering and Design* **163** (1996) 1-23.
12. A. Guelfi, D. Bestion, M. Boucker, P. Boudier, P. Fillion, M. Grandotto, J-M. Hérard, E. Hervieu, P. Péturaud, "NEPTUNE - A new software platform for advanced nuclear thermal hydraulics", *Nuclear Science and Engineering*, vol. **156**, pp. 281-324, 2007.

13. A. Hasan, R.P. Roy, S.P. Kalra, "Experiments on subcooled flow boiling heat transfer in a vertical annular channel", *Int. J. Heat Mass Transfer*, Vol **33**, Issue 10, Pages 2285-2293 (1990)
14. M. Ishii M., "Thermo-fluid dynamic, theory of two phase », Eyrolles, collection de la direction des Etudes et recherches d'Electricité de France, 1975.
15. M. Ishii, "Two-fluid model for two-phase flow", *Multiphase Science and Technology*, Hewitt G.F., Delhay J.M., Zuber N. Eds., Vol. **5**, pp. 1-58 (1990).
16. N. Kurul and M.Z. Podowski, "Multidimensional effects in forced convection subcooled boiling", *Proceedings of the Ninth International Heat Transfer Conference Jerusalem, Israel, August (1990)*, pp. 21–26 (1990).
17. M. Lance, M. Lopez de Bertodano, "Phase distribution phenomena and wall effects in bubbly two-phase flows", *Multiphase Science and Technology*, Vol. **8**, Hewitt G.F., Kim J.H., Lahey R.T. Jr., Delhay J.M. & Zuber N., Eds, Begell House, pp. 69-123 (1994).
18. J-M. Le Corre, S-C. Yao, C.H. Amon, "A mechanistic model of critical heat flux under subcooled flow boiling conditions for application to one- and three-dimensional computer codes", *Nuclear Engineering and Design* **240** (2010) 235-244.
19. C.H. Lee, J. Mudawwar, "A mechanistic critical heat flux model for subcooled flow boiling based on local bulk conditions", *Int. J. Multiphase Flow*, vol **14** no 6 (1988), 711-728.
20. T.J. Liu, G. Bankoff, "Structure of air-water bubbly flow in a vertical pipe: II – void fraction, bubble velocity and bubble size distribution", *Int. J. Heat Mass Transfer* Vol **36**, Issue 4, pp1061-1072 (1993)
21. E. Manon, "Contribution à l'analyse et à la modélisation locale des écoulements bouillants sous-saturés dans les conditions des Réacteurs à Eau sous Pression", PhD thesis, Ecole Centrale Paris, (2000), in french.
22. S. Mimouni, M. Boucker, J. Laviéville, A. Guelfi, D. Bestion, "Modeling and computation of cavitation and boiling bubbly flows with the NEPTUNE_CFD code", *Nucl. Eng. And Design* **238** (2008) pp 680-692.
23. S. Mimouni, F. Archambeau, M. Boucker, J. Laviéville, C. Morel, "A second order turbulence model based on a Reynolds stress approach for two-phase flow – Part I : adiabatic cases", *Science and Technology For Nuclear Installations*, Volume 2009 (2009), Article ID 792395, 14 pages doi:10.1155/2009/792395.
24. S. Mimouni, F. Archambeau, M. Boucker, J. Lavieville, C. Morel, "A second order turbulence model based on a Reynolds Stress approach for two-phase boiling flow. PART 1 : Application to the ASU annular channel case", *Nuclear Engineering and Design*, Volume **240**, Issue 9, September 2010, Pages 2233-2243.
25. S. Mimouni, F. Archambeau, M. Boucker, J. Lavieville, C. Morel, "A second order turbulence model based on a Reynolds Stress approach for two-phase boiling flow and application to fuel assembly analysis", *Nuclear Engineering and Design*, Volume **240**, Issue 9, September 2010, Pages 2225-2232.
26. S. Mimouni, J. Lavieville, N. Seiler, P. Ruyer, "Combined evaluation of second order turbulence model and polydispersion model for two-phase boiling flow and application to fuel assembly analysis", *Nuclear Engineering and Design*, Volume **241**, Issue 11, November 2011, Pages 4523-4536.
27. S. Mimouni et al., "computational multi-fluid dynamics predictions of critical heat flux in boiling flow", submitted to *Nucl Eng and Design*, 2014.
28. B. Ramstorfer, H. Breitschadel, G. Steiner, "Modelling of the near-wall liquid velocity field in subcooled boiling flow", *Proceedings of the ASME Summer Heat Transfer Conference San Francisco, CA, July (2005) HT2005-72182* (2005).
29. R.P. Roy, V. Velidandla, S.P. Kalra, P. Péturaud, "Local measurements in the two-phase boiling region of turbulent subcooled boiling flow", *ASME Journal of Heat Transfer*, 1993.
30. P. Ruyer, N. Seiler, M. Beyer, F.P. Weiss, "A bubble size distribution model for the numerical simulation of bubbly flows", *6th International Conference on Multiphase Flow, ICMF . Leipzig, Germany, July 9-13* (2007).
31. A. Tomiyama, "Struggle with computational bubble dynamics", *3rd Int. Conf. Multiphase Flow ICMF'98, Lyon, France, June 8-12* (1998).

32. H.C. Unal, "Void fraction and incipient point of boiling during the subcooled nucleate flow boiling of water", *International Journal of Heat and Mass Transfer* **20** (1977), 409-419.
33. J. Weisman, B.S. Pei, "Prediction of critical heat flux in flow boiling at low qualities", *Int. J. Heat Mass Transfer*, vol. **26** no 10 (1983), 1463-1476.
34. N. Zuber, "On the dispersed two-phase flow in the laminar flow regime", *Chem. Eng. Sc.*, No. **19**, p. 897 (1964).